1

2

3   **BPIFB3 facilitates flavivirus infection by controlling RETREG1-dependent**

4   **reticulophagy**

5

6   Azia S. Evans[1,2], Nicholas J. Lennemann[1,2], Ka man Fan[1,2,3], and Carolyn B. Coyne[1,2*]

7

8   [1]Department of Pediatrics, University of Pittsburgh School of Medicine, [2]Center for Microbial
9   Pathogenesis, Children's Hospital of Pittsburgh of UPMC, Pittsburgh, PA 15219, [3] Tsinghua
10   University School of Medicine, Beijing, China
11
12
13

14   Running title: BPIFB3 regulates reticulophagy

15

16   Author contributions:

17   Azia S. Evans: Conceptualization, Investigation, Visualization, Writing- original draft preparation,
18   Writing- review and editing
19   Nicholas J. Lennemann: Conceptualization, Methodology, Writing- review and editing
20   Ka man Fan: Resources
21   Carolyn B. Coyne: Conceptualization, Funding acquisition, Supervision, Visualization, Writing-
22   review and editing
23

24

25

26

27   *Address correspondence:
28
29   Carolyn Coyne, PhD
30   9116 Rangos Research Center
31   Children's Hospital of Pittsburgh of UPMC
32   One Children's Hospital Way
33   4401 Penn Avenue
34   Pittsburgh, PA 15224
35   Phone (412) 692-7519
36   Email coynec2@pitt.edu

Abstract

The *flavivirus* genus, which includes dengue virus (DENV) and Zika virus (ZIKV), are significant human pathogens and the prevalence of infected vectors continues to geographically expand. Both DENV and ZIKV rely on expansion of the endoplasmic reticulum (ER) and the induction of autophagy to establish a productive viral infection. However, little is known regarding the interplay between the requirements for autophagy initiation during infection and the mechanisms used by these viruses to avoid clearance through the autophagic pathway. We recently showed that DENV and ZIKV inhibit reticulophagy (specific degradation of the ER through autophagy) by cleaving reticulophagy regulator 1 (RETREG1), an autophagy receptor responsible for targeted ER sheet degradation. These data suggest that DENV and ZIKV require specific autophagic pathways for their replication, while other autophagic pathways are antiviral. We previously identified BPI Fold Containing Family B Member 3 (BPIFB3) as a regulator of autophagy that negatively controls enterovirus replication. Here, we show that in contrast to enteroviruses, BPIFB3 functions as a positive regulator of DENV and ZIKV infection and that its RNAi-mediated silencing drastically inhibits the formation of viral replication organelles. We show that BPIFB3 depletion enhances ER fragmentation, while its overexpression protects against autophagy-induced ER degradation, demonstrating that BPIFB3 serves as a specific regulator of ER turnover. We further show that the antiviral effects of BPIFB3 depletion on flavivirus infection are reversed in RETREG1-depleted cells, and that BPIFB3 associates with RETREG1 within the ER, suggesting that BPIFB3 regulates a RETREG1-specific reticulophagy pathway. Collectively, these studies identify BPIFB3 as a regulator of the reticulophagy pathway and define the requirements for a novel host regulator of flavivirus infection.

Author Summary

Flaviviruses and other arthropod transmitted viruses represent a widespread global health problem with limited treatment options currently available. Thus, greater knowledge of the host

2

63   factors required for replication and transmission is needed to provide a better understanding of

64   the cellular requirements for infection. Here, we show that the endoplasmic reticulum (ER)

65   localized protein, BPIFB3 is required to facilitate flavivirus infection. Depletion of BPIFB3 in cells

66   inhibits dengue virus and Zika virus infection prior to replication of the viral genome.

67   Mechanistically, we show that BPIFB3 inhibits ER degradation in an autophagy-specific manner

68   and that loss of BPIFB3 decreases the availability of ER membranes needed for flavivirus

69   replication. We further show that BPIFB3 specifically regulates the RETREG1 pathway, but not

70   other pathways of ER turnover. Together, our data define a previously uncharacterized method

71   of regulating ER degradation and show that BPIFB3 is an essential host factor for a productive

72   flavivirus infection.

73

74   **Introduction**

75   Flaviviruses, which include dengue virus (DENV) and Zika virus (ZIKV), are enveloped,

76   positive-sense RNA viruses that replicate exclusively within endoplasmic reticulum (ER)

77   membranes (1,2). Upon entry and uncoating, the flaviviral genome is directly translated as a

78   single polyprotein and embedded in the ER, which induces ER expansion and the formation of

79   viral replication organelles (3–6). Like other RNA viruses, flaviviruses sequester their replication

80   machinery within membrane bound compartments that provide a high concentration of host and

81   viral replication factors, while isolating viral replication intermediates from detection by the host

82   innate immune system (7,8).

83   The success of flavivirus replication is closely linked to the availability of ER membranes.

84   The ER is an expansive network of membranous sheets and tubules that originate at the nuclear

85   envelope and extend to the cell periphery (9). ER sheets are distributed perinuclearly and function

86   as the primary location of protein synthesis, while ER tubules extend to the plasma membrane

87   and play a prominent role in lipid synthesis and communication with other organelles (10). Both

88   DENV and ZIKV utilize rough ER as the primary source of membranes for the formation of

89   replication organelles, while smooth ER is used in the formation of convoluted membranes during

90   viral replication (7). These convoluted membranous formations are found in close proximity to

91   replication complexes and mitochondria, suggesting a role in lipid synthesis and/or membrane

92   expansion during infection (8).

93   Although autophagy commonly serves as a proviral pathway for RNA viruses, these

94   viruses often avoid clearance by flux through the autophagic pathway, which can function in an

95   antiviral manner (11). In the absence of infection, macroautophagy, hereafter referred to as

96   autophagy, functions to degrade bulk cytoplasmic contents and excess or damaged organelles

97   by fusion with the lysosome, which is referred to as autophagic flux (12,13). During infection,

98   autophagy functions as an innate defense pathway to facilitate the clearance of viral complexes

99   and infectious particles (14–16). Furthermore, recent evidence suggests that autophagy can be

100   specifically activated through innate immune signaling to induce the clearance of intracellular

101   pathogens (17). To overcome autophagy-mediated clearance, many viruses have developed

102   strategies to either inhibit flux through the autophagic pathway or to utilize it in a proviral manner

103   for virion maturation and release (14). However, the full relationship between flaviviruses and

104   autophagy remains unclear. Evidence suggests that DENV and ZIKV induce autophagy as a

105   mechanism to promote viral infection (18,19). Specifically, DENV infection promotes the

106   degradation of lipid droplets by autophagy, termed lipophagy, to allow for an increased energy

107   supply during infection (20,21). In contrast, we have previously demonstrated that degradation of

108   the ER through selective autophagy (reticulophagy) restricts flavivirus replication due to the

109   dependence of viral replication on ER membranes (22). Furthermore, DENV and ZIKV specifically

110   inhibit reticulophagy by cleaving reticulophagy regulator 1 (RETREG1), which is necessary for

111   targeted ER sheet degradation (22). These studies collectively suggest that specific autophagic

112   pathways may be anti-flaviviral, while others are pro-flaviviral.

113   We previously identified bactericidal/permeability increasing protein (BPI) fold containing

114   family B member 3 (BPIFB3) as an ER-localized antiviral regulator of coxsackievirus B (CVB)

4

115   infection, a positive-sense RNA virus belonging to the *Enterovirus* genus, through its negative

116   regulation of a non-canonical form of autophagy (23). Similar to flaviviruses, CVB relies on the

117   availability of intracellular membranes to establish replication compartments; however, the source

118   of these cellular membranes is variable. In this study, we identified BPIFB3 as a positive regulator

119   for flavivirus infection. Mechanistically, we show that BPIFB3 functions upstream of RETREG1 to

120   specifically control reticulophagy, thereby controlling the availability of ER membranes for viral

121   replication. Our study therefore defines a specific role for BPIFB3 in reticulophagy and suggests

122   that it differentially controls enterovirus and flavivirus replication.

123

124   **Results**

125   **BPIFB3 is required for DENV and ZIKV infection**

126   We have previously shown that BPIFB3 is an ER-localized negative regulator of CVB infection

127   (23). Given that flaviviruses replicate exclusively on membranes derived from the ER, we

128   determined whether BPIFB3 also functions to regulate DENV and ZIKV replication. To do this,

129   human brain microvascular endothelial cells (HBMEC) were transfected with either a siRNA

130   targeting BPIFB3 (BPIFB3si) or a control siRNA (CONsi) and infected with DENV, ZIKV, or CVB

131   (23). In contrast to the significant enhancement of CVB infection, RNAi-mediated silencing of

132   BPIFB3 resulted in an approximately 90% decrease in the replication of both DENV and ZIKV, as

133   assessed by RT-qPCR and immunofluorescence microscopy for the production of double-

134   stranded RNA, a replication intermediate (**Figure 1a, d, S1d**), and a 100-fold decrease in

135   infectious particle production (**Figure 1b**). This phenotype was specific for BPIFB3 and other

136   members of the BPIFB family (BPIFB2 and BPIFB6) did not affect DENV and ZIKV uniformly

137   (**Figure S1a, b)**. Depletion of BPIFB3 was confirmed by RT-qPCR (**Figure S1c**). To determine at

138   which stage of the flaviviral life cycle BPIFB3 depletion impairs, we used HBMEC stably

139   propagating a DENV subgenomic replicon (HBMEC^{rep}) (24). DENV replicon cells express the full

140   seven nonstructural proteins that allows for replication of replicon RNA as well as the remodeling

5

141   of ER membranes, including the formation of replication organelles, similar to viral infection (25).

142   Silencing of BPIFB3 in HBMEC^{rep} had no effect on replicon RNA levels (**Figure 1c**), suggesting

143   the defect in flavivirus infection occurs prior to the formation of viral replication organelles within

144   the ER.

145   To characterize the effects of BPIFB3 depletion on DENV and ZIKV infection, we

146   performed transmission electron microscopy (TEM) on DENV- and ZIKV-infected HBMEC

147   transfected with CONsi or BPIFB3si. We found that BPIFB3si prevented the formation of both

148   DENV and ZIKV membrane bound viral replication organelles (**Figure 1e**). Quantification of ZIKV

149   replication organelles (defined as ER associated, membrane bound vesicles of approximately 70-

150   100 nm) confirmed that BPIFB3 silencing inhibited flavivirus infection prior to genome replication

151   (**Figure 1f**). In addition to defects in replication organelle formation, we did not observe the

152   formation of convoluted membranes or ER rearrangement characteristic of flavivirus infection in

153   BPIFB3-depleted cells, suggesting BPIFB3si inhibits infection early during the viral lifecycle.

154

155   **Infection of BPIFB3 depleted cells induces aberrant ER structures**

156   We showed previously that BPIFB3 localizes to domains enriched for the ER sheet marker

157   CLIMP63 (26). Therefore, we sought to examine whether BPIFB3 is involved in regulating ER

158   morphology or turnover during flavivirus infection. In uninfected cells, ER sheets originate at the

159   nuclear envelope and extend to the cell periphery in a fairly uniform arrangement; however, during

160   infection with DENV and ZIKV, ER sheets (marked by CLIMP63) condense around the perimeter

161   of the nucleus where they co-localize with viral double stranded RNA (dsRNA), designating the

162   location of viral membrane remodeling and replication organelle formation (22). In some cases,

163   cells depleted of BPIFB3 exhibited low levels of viral replication (as determined by dsRNA

164   immunofluorescence); however, these cells exhibited an abnormal rearrangement of CLIMP63-

165   positive ER domains into punctate structures (**Figure 2a**). The ability to establish infection in

166   select BPIFB3si cells may be caused by variations in knockdown efficiency across individual cells,

6

167   or could indicate that in some cases, low levels of replication can be initiated in cells depleted of

168   BPIFB3. TEM analysis of BPIFB3 depleted cells infected with ZIKV exhibited dramatic expansions

169   of ER membranes with no evidence of replication organelles (**Figure 2b**). Importantly, uninfected

170   BPIFB3si transfected cells did not exhibit aberrant ER structures and contained few identifiable

171   ER membranes; suggesting that ZIKV may be able to infect BPIFB3 depleted cells and induce

172   early ER remodeling but is unable to readily form replication organelles or establish efficient

173   replication.

174

175   **BPIFB3 regulates ER sheet morphology in response to autophagy induction**

176   We previously demonstrated that BPIFB3 serves as a regulator of a non-canonical form of

177   autophagy, however the precise mechanism of regulation remained unclear (23). To assess the

178   impact of BPIFB3 silencing on host cell pathways, we performed whole transcriptome RNAseq

179   studies on uninfected and infected HBMEC transfected with CONsi or BPIFB3si. Differential

180   expression analysis identified numerous autophagy related genes as dysregulated in BPIFB3si

181   samples compared to controls (**Figure 3a**). These included ATG101, WIPI3, ATG3, ATG12, and

182   LC3B which were transcriptionally upregulated in BPIFB3 depleted cells and are involved in

183   autophagosome formation prior to vesicle release and maturation (12). Interestingly, WIPI2,

184   BECN1, ATG10, and ATG7 were downregulated in BPIFB3si cells despite their function during

185   autophagosome formation in conjunction with the upregulated genes mentioned above. These

186   results further suggested that BPIFB3 is involved in regulating a non-canonical form of autophagy.

187   Importantly, our transcriptional analyses did not reveal an increase in interferons (IFNs) or

188   interferon stimulated gene (ISG) production in uninfected or infected samples, confirming that the

189   decrease in infection observed in BPIFB3 depleted cells is not the result of increased innate

190   immune activation or signaling. We also examined the expression levels of ER structural

191   transcripts and found that the ER sheet marker CLIMP63 (also named CKAP4) was upregulated

192   in uninfected BPIFB3si samples, while the ER tubule protein reticulon3 (RTN3) was

7

193   downregulated. These transcriptional changes may suggest a need for increased ER sheet

194   production in response to BPIFB3 silencing.

195   Given that we observed an enhancement in ER-enriched punctae in DENV and ZIKV

196   infected BPIFB3si cells (**Figure 2a**), we next determined whether BPIFB3 enhanced ER

197   degradation through autophagy. To do this, we examined ER sheet morphology by

198   immunofluoresence under both nutrient rich (fed) or serum starved conditions, which induces

199   autophagy. We found that serum starvation of cells depleted of BPIFB3 induced the formation of

200   CLIMP63 puncta that were absent in CONsi transfected cells (**Figure 3b**). To determine if this

201   was unique to ER sheets, or if BPIFB3si also influenced the rearrangement of ER tubules, we

202   analyzed the localization of the tubule specific protein reticulon4 (RTN4). Serum starvation

203   induced the rearrangement of RTN4 positive ER tubules, however this phenotype was also

204   observed in CONsi cells, and was not further exaggerated by BPIFB3 depletion (**Figure S2**).

205   To determine if ectopic expression of BPIFB3 exerted an opposing phenotype leading to

206   the stabilization of ER sheets, we transfected human osteosarcoma U2OS cells with V5 fused

207   BPIFB3 (BPIFB3-V5) and transferred them to either nutrient rich media (fed) or HBSS (serum

208   starved) 48 hours post transfection. Using quantitative image analysis, we found that the levels

209   of endogenous CLIMP63 were significantly higher in cells overexpressing BPIFB3 under both

210   conditions (**Figure 3c, 3d**). These data suggest that BPIFB3 expression protects ER sheets from

211   degradation through autophagy, and that loss of BPIFB3 leads to enhanced ER turnover.

212

213   **RETREG1 and BPIFB3 localize in close proximity within the ER**

214   Given our data indicating BPIFB3 stabilizes ER sheets, we sought to determine whether BPIFB3

215   regulates the reticulophagy pathway. We first analyzed whether BPFIB3 localizes with RETREG1,

216   which we showed previously functions as an antiviral regulator of flavivirus infection (22).We

217   found that ectopically expressed BPIFB3 colocalized with both wild-type RETREG-1 and an

218   autophagy deficient mutant of RETREG1 lacking an LC3 interacting region (LIR) (mutLIR),

8

219   suggesting that BPIFB3 and RETREG1 colocalize independent of the ability of RETREG-1 to

220   function in reticulophagy (**Figure 4a**). To assess if co-localization was due to a direct interaction

221   we performed co-immunoprecipitation experiments, however we were unable to observe an

222   interaction between BPIFB3 and RETREG1 due to low protein solubility.

223   To determine whether BPIFB3 and RETREG1 reside in close proximity to one another,

224   we used a modified reversible bimolecular fluorescence complementation (BiFC) assay. This

225   assay utilizes GFP broken into two distinct fragments, a large portion composed of the first ten β

226   sheets of GFP (GFP1-10) and a smaller fragment composed of the eleventh β sheet (GFP11)

227   (27). When the tagged proteins do not interact or associate within the same complex, the GFP

228   fragments are too far apart and there is no fluorescence. However, if there is either a direct or

229   indirect association (of less than 10nm apart), GFP folds correctly and fluoresces similar to full

230   length GFP (28) (schematic, **Figure 4b**). We fused RETREG1 with GFP1-10 and BPIFB3 with

231   the smaller GFP11. U2OS cells were transfected with each split GFP construct and with either

232   mCherry fused CLIMP63 or RFP fused LC3. We found that RETREG1 GFP1-10 and BPIFB3

233   GFP11 localized in very close proximity (<10nm) to one another, as determined by positive GFP

234   fluorescence in cotransfected cells, however no green fluorescence was observed when

235   RETREG1 GFP1-10 was expressed with GFP11 alone (**Figure S3**). We further found that BiFC-

236   component BPIFB3 and RETREG1 co-localized with the ER sheet marker CLIMP63, but not the

237   autophagosome marker LC3 (**Figure 4c**). These data suggest that BPIFB3 and RETREG1

238   localize to ER sheets and are in close proximity, but may not form a direct interaction. Further, we

239   did not observe RETREG1 colocalization with LC3B upon expression of BPIFB3, thus BPIFB3

240   may restrict RETREG1-mediated reticulophagy.

241

242   **BPIFB3 negatively regulates RETREG1-mediated reticulophagy**

9

243   To determine whether silencing of BPIFB3 enhances reticulophagy, we first analyzed ER

244   morphology and autophagosome accumulation by TEM in cells co-depleted of BPIFB3 and

245   RETREG1. We previously showed that BPIFB3 silencing leads to an accumulation of

246   autophagosomes, lysosomes, and amphisomes (23). However, this phenotype was completely

247   reversed in cells transfected with RETREG1si (**Figure 4d, 4e**), suggesting that this induction

248   occurs downstream of RETREG-1-mediated reticulophagy.

249   In response to autophagy induction, RETREG1 interacts with LC3 to target ER

250   membranes to the autophagosome for eventual degradation by the lysosome (13). Given that

251   BPIFB3 expression led to increased levels of ER sheets and that silencing of RETREG1 reversed

252   the induction of autophagy in cells transfected with BPIFB3si, our data suggested that BPIFB3

253   inhibits RETREG1-mediated reticulophagy. To confirm this, we transfected U2OS cells with

254   RETREG1-GFP and LC3-RFP in the presence or absence of BPIFB3 under nutrient rich or

255   nutrient deprived conditions. We found no differences in the numbers of RETREG1 positive

256   puncta alone (**Figure 5b**) or in the co-localization of RETREG1 and LC3 puncta (**Figure 5c**) under

257   nutrient rich conditions. However, in response to nutrient deprivation, we found that BPIFB3

258   expression significantly reduced the number or RETREG1 positive puncta (**Figure 5b**) and

259   prevented the co-localization of RETREG1 with LC3 (**Figure 5c**). Collectively, these data suggest

260   that BPIFB3 functions as a negative regulator of RETREG1-mediated reticulophagy.

261

262   **BPIFB3 facilitates flavivirus replication by negatively regulating reticulophagy**

263   DENV and ZIKV are dependent on the availability of ER membranes to replicate and

264   reticulophagy thus functions as an antiviral pathway that limits the availability of these membranes

265   (22). To determine if the reduction of flavivirus replication in cells depleted of BPIFB3 resulted

266   from enhanced reticulophagy, we co-depleted BPIFB3 and RETREG1 in cell and infected with

267   DENV or ZIKV. We found that silencing of RETREG1 completely reversed the inhibition of

268   flavivirus infection in cells silenced for BPIFB3 expression, as determined by both qPCR for vRNA

10

269   and FFU for viral titers (**Figure 6a, 6b**). Consistent with our previous work (22), silencing of

270   RETREG1 enhanced flavivirus replication, which was unaffected by BPIFB3 silencing. Moreover,

271   we found that co-depletion of BPIFB3 and RETREG1 also reversed the proviral impact of BPIFB3

272   silencing on CVB replication (**Figure 6c**). Depletion of BPIFB3 and RETREG1 was confirmed by

273   RT-qPCR (**Figure S4**). Interestingly, we found that BPIFB3 specifically regulates RETREG1-

274   mediated ER sheet reticulopahgy as the anti-flaviviral effect of BPIFB3 silencing was unaffected

275   by silencing of either reticulon 3 (RTN3), the ER tubule specific reticulophagy receptor, or the ER

276   stress-specific reticulophagy receptor Sec62 (**Figure S5**). Lastly, we found that BPIFB3 localizes

277   to the same ER domains as flaviviral nonstructural proteins during active replication, as

278   determined by the colocalization of DENV NS1, NS3 and ZIKV NS4B which localize to replication

279   organelles during infection (**Figure 6d**). These data implicate BPIFB3 as a specific negative

280   regulator of RETREG1-mediated reticulophagy, which functions to promote flaviviral replication.

281

282   **Discussion**

283   The success of flavivirus infection depends on the cooperation of numerous cellular

284   organelles and pathways that function to produce progeny virions, specifically relying on host

285   membranes throughout their lifecycles. Here we show that BPIFB3 is required for DENV and ZIKV

286   infection by regulating the availability of ER membranes for viral remodeling. Our data show that

287   BPIFB3 depletion enhances ER sheet reticulophagy in response to viral infection and the

288   induction of autophagy. Furthermore, we demonstrate BPIFB3 functions to regulate RETREG1

289   targeted reticulophagy and not RTN3 or Sec62 specific pathways. These findings thus not only

290   define the role of specific autophagic pathways in the regulation of flavivirus infection, but also

291   identify BPIFB3 as a novel regulator of RETREG1-specific forms of reticulophagy.

292   Unlike other RNA viruses, flaviviruses depend solely on ER-derived membranes for their

293   replication. The viral genome is delivered to the rough ER following entry and uncoating, where

294   translation of viral proteins induces expansion of the ER. Of the seven nonstructural proteins, the

11

295   majority remain associated with the ER throughout the lifecycle, where they function in viral

296   replication, membrane remodeling, and inactivation of reticulophagy and ER stress pathways (5–

297   7,22,29,30). While it has been suggested that the virally-encoded non-structural proteins NS1,

298   NS4A, and NS4B are involved in membrane manipulation during DENV infection, little is known

299   regarding host factors essential for this process. Currently, only three host factors have been

300   implicated in membrane expansion, including fatty acid synthase, RETREG1, and reticulon 3.1A

301   (RTN3.1A). FASN is recruited to sites of replication organelle formation by the DENV protease

302   NS3, suggesting increased lipid synthesis is important for membrane remodeling (20).

303   Additionally, both DENV and ZIKV inhibit ER degradation by cleaving the RETREG1

304   reticulophagy receptor, allowing for an accumulation of ER membranes (22). Lastly, RTN3.1A

305   localizes to viral replication organelles to facilitate proper membrane curvature, however it does

306   not interact with DENV or ZIKV NS4a during membrane remodeling (31). Our work presented

307   here further confirms that degradation of the ER is an antiviral process and defines a new

308   mechanism used by flaviviruses to regulate ER turnover. RNAi mediated silencing of BPIFB3

309   leads to enhanced levels of reticulophagy, which decreases the availability of ER membranes for

310   flavivirus replication. Concurrent depletion of RETREG1 with BPIFB3 overcomes this defect,

311   demonstrating that the antiviral effects of BPIFB3 depletion are specific to RETREG1-mediated

312   reticulophagy and inhibition of this pathway restores viral replication. These data imply that the

313   manipulation of BPIFB3 protein levels during flavivirus infection could alter reticulophagy levels

314   to either enhance viral replication or allow for the host cell to overcome infection at an early stage.

315   One method proposed to promote membrane expansion during flavivirus infection is the

316   induction of autophagy (30). However, our data demonstrate that enhanced levels of

317   reticulophagy, particularly early during infection, inhibits membrane remodeling and replication

318   organelle formation. Recent work has identified a number of ER-specific autophagy pathways that

319   differ by the receptor used to target cargo to autophagosomes (13,32,33). However, it remains

320   unclear whether these pathways are regulated by the same machinery that controls canonical

12

321 macroautophagy. The growing diversity in the various forms of autophagy further complicates our

322 understanding of the relationship between viral infection and this pathway, as certain forms of

323 autophagy may differentially regulate viral replication at various stages of the viral life cycle. The

324 work presented here, in combination with our previous work characterizing BPIFB3 as a negative

325 regulator of CVB infection, demonstrates the unique requirements for autophagy between

326 different RNA virus families. In contrast to the unclear role for distinct autophagic pathways in

327 flavivirus infection, CVB benefits from autophagy induction, as it uses autophagosomes and other

328 cytoplasmic vesicles for replication organelle formation. Importantly, CVB inhibits fusion of the

329 autophagosome with the lysosome, which enhances the number of cytoplasmic vesicles and

330 prevents the degradation of viral replication machinery (34–36). Conversely, it has not been

331 demonstrated whether flaviviruses have developed strategies to avoid clearance through the

332 macroautophagy pathway similar to CVB and other enteroviruses. While the induction of

333 autophagy during flavivirus infection has been implicated in enhancing viral replication (37), the

334 precise timing of induction may have distinct effects on the viral lifecycle. Furthermore, the ability

335 to specifically activate one form of autophagy while inhibiting others may be essential for

336 successful flavivirus infection. The distinction between membrane manipulation during CVB

337 infection and flavivirus infection explains the differential effects of BPIFB3 in regulating these

338 unique viruses and further suggests that increased flux through autophagy is detrimental to

339 flavivirus replication.

340   The BPIFB family of proteins were initially named and identified because of their homology

341 to the bactericidal/permeability-increasing (BPI) protein; a secreted antimicrobial protein that

342 functions through binding to LPS (38–40). Despite the high degree of predicted structural

343 homology, BPIFB3 localizes to the ER and is not secreted (23). Of the other members of the

344 family, BPIFB2 and BPIFB6 are also ER localized, however neither appear to regulate autophagy

345 (26) or flavivirus infection. BPIFB proteins contain two BPI folds demonstrated to have lipid

346 binding properties. Unlike other BPIFB proteins, the first BPI domain (BPI1) of BPIFB3 lacks the

13

347   ability to bind lipids, while BPI2 is capable of binding phosphatidic acid, phosphatidyserine,

348   cardiolipin, and other lipid molecules (26). Of the related proteins, BPIFB6 is the only protein to

349   be characterized, and has been demonstrated to regulate secretory trafficking and Golgi

350   morphology (26). Together with the data presented here, this suggests that a possible unifying

351   function of these proteins is to regulate sites of vesicle trafficking. Here we show BPIFB3 over

352   expression decreases the amount of ER specific autophagosomes in a cell, while depletion

353   enhances reticulophagy. In comparison, BPIFB6 depletion results in Golgi dispersal and a

354   disruption of retrograde and anterograde trafficking (26). This alludes to a possible mechanism

355   where BPIFB3 and BPIFB6 expression is associated with decreased vesicle trafficking to the

356   autophagic and secretory pathways respectively, while loss of expression leads to enhanced

357   vesicle trafficking originating in the ER. Importantly, expression of BPIFB3 is remarkably low, and

358   we are unable to detect endogenous protein by either western or immunofluorescence. Despite

359   its low expression, depletion of BPIFB3 elicits a dramatic phenotype in cells, suggesting an

360   essential role in regulating morphology of the cellular membrane network. This is consistent with

361   other ER structural proteins that drastically effect membrane morphology at very low levels of

362   endogenous expression (41). Their potential roles in vesicle trafficking has important implications

363   for the ability of these proteins to impact the trafficking and spread of a variety of viruses. However,

364   further characterization is required to delineate the different methods by which viruses are

365   trafficked during infection.

366   The relationship between flavivirus infection and the autophagic pathway is likely to be

367   complex. While the initiation of autophagy and lipophagy have been demonstrated as proviral

368   pathways (19,21,30,37), flux through the autophagic pathway and reticulophagy are antiviral

369   (18,22,42). Thus, further characterization of the role of specific autophagic pathways in the

370   regulation of flavivirus infection is needed to understand and develop new mechanisms to control

371   infection.

372

14

373 **Methods**

374 **Cells and viruses**

375 Human brain microvascular endothelial cells (HBMEC) were maintained in in RPMI 1640

376 supplemented with 10% fetal bovine serum (FBS), 10% NuSerum, 1x non-essential amino acids,

377 1x minimum essential medium vitamins, 1% sodium pyruvate, and 1% antibiotic. Human bone

378 osteosarcoma U2OS and Vero cells were grown in DMEM with 10% FBS and 1% antibiotic.

379 Development of DENV replicon HBMECs using constructs provided by Theodore Pierson

380 (NIH/NIAID) was described previously(24). *Aedes albopictus* midgut C6/36 cells were cultured in

381 DMEM supplemented with 10% FBS and 1% antibiotic at 28°C in a 5% CO_2 atmosphere.

382   DENV2 16881 and ZIKV Paraiba/2015 (provided by David Watkins, University of Miami)

383 were propagated in C6/36 or Vero cells, respectively(43). Titers were determined by fluorescent

384 focus assay as previously described, using recombinant anti-double-stranded RNA monoclonal

385 antibody (provided by Abraham Brass, University of Massachusetts)(44). Propagation and

386 titration have been describe previously of CVB3 (RD) has been described previously(45).

387 Experiments measuring infection levels were performed using a multiplicity of infection (MOI) of

388 1 for 16 hours (CVB) or 48 hours (DENV and ZIKV), and infection was quantified by RT-qPCR or

389 fluorescent focus assay.

390

391 **siRNAs, plasmids and transfections**

392 Characterization of siRNAs targeting BPIFB3, BPIFB2, BPIFB6, and RETREG1 (FAM134B) have

393 been described previously(22,23). Sequences of siRNAs targeting RTN3 or Sec62 are, RTN3:

394 CCACUCAGUCCCAUUCCAUtt, and Sec62: GAAGGAUGAGAAAUCUGAAtt. All siRNAs,

395 including the scrambled control (CONsi), were purchased from Sigma. Efficiency of knockdown

396 was determined by RT-qPCR for each siRNA target. siRNAs were reverse transfected at 25 nM

397 in to HBMEC using Dharmafect 1, and cells were either infected or RNA was collected 48 hrs post

398 transfection.

15

399   V5 -fused BPIFB3 was generated by cloning into pcDNA3.1/V5-His TOPO TA according

400   to the manufacturer's protocol. Development of GFP tagged RETREG1 and RETREG1mutLIR

401   have been described elsewhere(22). RETERG1 GFP1-10 and BPIFB3 GFP11 were cloned into

402   pcDNA3.1-GFP(1-10) or pEGFP-GFP11 respectively, using plasmids provided by Seema

403   Lakdawala (University of Pittsburgh). RFP tagged LC3 cloning has been described previously(46).

404   Plasmids were reverse transfected into U2OS cells using either X-tremeGENE 9 or X-tremeGENE

405   HP according to the manufacturers protocol and fixed for fluorescence microscopy or infected at

406   48 hrs post transfection.

407

408   **RNA extraction, cDNA synthesis, and RT-qPCR**

409   RNA was isolated using the GenElute Total RNA MiniPrep kit from Sigma according to the kit

410   protocol. RNA was reverse transcribed using the iScript cDNA Synthesis kit (Bio-Rad) with $1\mu g$

411   of RNA per sample. RT-qPCR was performed using IQ SYBR green SuperMix (Bio-Rad) in a Bio-

412   Rad CFX96 Touch real-time PCR detection system. A modified threshold cycle (ΔCT) method

413   was used to calculate gene expression using human actin for normalization. Primer sequences

414   for actin, DENV, ZIKV, CVB, BPIFB3, and RETREG1 have been described previously(22,46).

415

416   **RNAseq**

417   Total RNA was isolated as described above, and RNAseq was performed as previously

418   described(25). Analysis of RNAseq data sets was performed using CLC Genomics 11 (Qiagen)

419   to process and map sequences to the human genome (hg19) or the appropriate viral genome to

420   calculate viral fragments per kilobase of transcript per million mapped reads (FPKM) values.

421   Differentially expressed genes were identified using the DeSeq2 package in R with a significance

422   cutoff of 0.001 and a fold change cutoff of two(47). Gene set enrichment analysis (GSEA) and

423   manual sorting were used to identify pathways or specific transcripts differentially regulated.

424   Generation of heat maps was done using MeViewer software based on ln(RPKM) values.

16

425

Antibodies

427   Mouse monoclonal anti-V5 epitope tag was purchased from Invitrogen (R960-25). Rabbit

428   polyclonal antibodies against CKAP4 (16686-1-AP), RTN4 (10950-1-AP), and FAM134B (21537-

429   1- AP) were purchased from ProteinTech. Rabbit polyclonal antibodies to DENV NS3

430   (GTX124252) and ZIKV NS4B (GTX133311) were purchased from GeneTex. Recombinant

431   mouse monoclonal anti-dsRNA was provided by Abraham Brass (University of Massachusetts).

432   Alexa Fluor conjugated secondary antibodies were purchased from Invitrogen.

433

Immunofluorescence and electron microscopy

435   Immunofluorescence microscopy was performed on cells grown in 8-well chamber slides

436   (company?), fixed in 4% paraformaldehyde, and permeabilized with 0.1% Triton. In some cases,

437   cells were fixed in ice cold methanol. Primary antibodies were incubated in PBS with cells for 1

438   hr, followed by staining with Alexa Fluor conjugated secondary antibodies for 30 min. Slides were

439   mounted with coverslips using VectaShield containing 40-6-diamino-2-phenylindole (DAPI).

440   Imaging was performed on an Olympus IX83 inverted microscope. All image quantification was

441   performed using ImageJ/FIJI. Pixel intensity measurements were performed using isolated

442   channels on individual cells with the region of interest (ROI) manager. Data are presented as

443   mean pixel intensity, normalized to cell area. Quantification of fluorescent puncta was performed

444   manually, counting the number ER localized vesicles alone, or co-localized with the indicated

445   marker. Preparation of samples for TEM were done as previously described, by the Center for

446   Biologic Imaging (University of Pittsburgh)(46). Imaging was performed on a JEOL 1011

447   transmission electron microscope. Quantification of TEM images was performed manually.

448

Statistical analyses

450   All analyses were performed using GraphPad Prism. Experiments were performed at least three

17

451 times. Student's t test, 2way analysis of variance (ANOVA), or one-way ANOVA were used where

452 indicated. Analysis of fluorescent microscopy data was done using a non-parametric Kruskal-

453 Wallis test. Data are presented as mean ± standard deviation, with specific p-values detailed in

454 the figure legends.

455

456 **Acknowledgements**

462

463 **References**

464 1.   Welsch S, Miller S, Romero-Brey I, Merz A, Bleck CKE, Walther P, et al. Composition

465   and Three-Dimensional Architecture of the Dengue Virus Replication and Assembly

466   Sites. Cell Host Microbe. 2009;5(4):365–75. Doi: 10.1016/j.chom.2009.03.007

467 2.   Cortese M, Goellner S, Acosta EG, Neufeldt CJ, Oleksiuk O, Lampe M, et al.

468   Ultrastructural Characterization of Zika Virus Replication Factories. Cell Rep.

469   2017;18(9):2113–23.

470 3.   Kaufusi PH, Kelley JF, Yanagihara R, Nerurkar VR. Induction of endoplasmic reticulum-

471   derived replication-competent membrane structures by West Nile virus non-structural

472   protein 4B. PLoS One. 2014;9(1).

473 4.   Miller S, Kastner S, Krijnse-Locker J, Bühler S, Bartenschlager R. The non-structural

474   protein 4A of dengue virus is an integral membrane protein inducing membrane

475   alterations in a 2K-regulated manner. J Biol Chem. 2007;282(12):8873–82.

476 5.   Peña J, Harris E. Early dengue virus protein synthesis induces extensive rearrangement

477   of the endoplasmic reticulum independent of the UPR and SREBP-2 pathway. PLoS One.

478   2012;7(6):1–15.

479 6.   Gillespie LK, Hoenen A, Morgan G, Mackenzie JM. The Endoplasmic Reticulum Provides

480   the Membrane Platform for Biogenesis of the Flavivirus Replication Complex. J Virol.

481   2010;84(20):10438–47. Doi: 10.1128/JVI.00986-10.

482 7.   Paul D, Bartenschlager R. Flaviviridae Replication Organelles: Oh, What a Tangled Web

483   We Weave. Annu Rev Virol. 2015;2(1):289–310. Doi: 10.1146/annurev-virology-100114-

484   055007.

485 8.   Neufeldt CJ, Cortese M, Acosta EG, Bartenschlager R. Rewiring cellular networks by

486   members of the Flaviviridae family. Nat Rev Microbiol. 2018;16(3):125–42. Doi:

487   10.1038/nrmicro.2017.170.

488 9.   Shibata Y, Shemesh T, Prinz WA, Palazzo AF, Kozlov MM, Rapoport TA. Mechanisms

489   determining the morphology of the peripheral ER. Cell. 2010;143(5):774–88. Doi.

490   10.1016/j.cell.2010.11.007.

491 10.   Lin S, Sun S, Hu J. Molecular basis for sculpting the endoplasmic reticulum membrane.

492   Int J Biochem Cell Biol. 2012;44(9):1436–43. DOI: 10.1016/j.biocel.2012.05.013.

493 11.   Lennemann NJ, Coyne CB. Catch Me If You Can: The Link between Autophagy and

494   Viruses. PLoS Pathog. 2015;11(3):1–6.

495 12.   Bento CF, Renna M, Ghislat G, Puri C, Ashkenazi A, Vicinanza M, et al. Mammalian

496   Autophagy: How Does It Work? Annu Rev Biochem. 2016;85(1):685–713. Doi:

497   10.1146/annurev-biochem-060815-014556.

498 13.   Khaminets A, Heinrich T, Mari M, Grumati P, Huebner AK, Akutsu M, et al. Regulation of

499   endoplasmic reticulum turnover by selective autophagy. Nature. 2015;522(7556):354–8.

500   Doi: 10.1038/nature14498.

501 14.   Kirkegaard K. Subversion of the cellular autophagy pathway by viruses. Current Topics in

502   Microbiology and Immunology. 2009.

19

503   15.   Levine B, Mizushima N, Virgin HW. Autophagy in immunity and inflammation. Nature.

504   2011;469(7330):323–35. Doi: 10.1038/nature09782.

505   16.   Deretic V, Saitoh T, Akira S. Autophagy in infection, inflammation and immunity. Nat Rev

506   Immunol. 2013;13(10):722–37. Doi: 10.1038/nri3532.

507   17.   Moretti J, Roy S, Bozec D, Martinez J, Chapman JR, Ueberheide B, et al. STING Senses

508   Microbial Viability to Orchestrate Stress-Mediated Autophagy of the Endoplasmic

509   Reticulum. Cell. 2017;171(4):809–823.e13. Doi: 10.1016/j.cell.2017.09.034.

510   18.   Metz P, Chiramel A, Chatel-Chaix L, Alvisi G, Bankhead P, Mora-Rodríguez R, et al.

511   Dengue Virus Inhibition of Autophagic Flux and Dependency of Viral Replication on

512   Proteasomal Degradation of the Autophagy Receptor p62. J Virol. 2015;89(15):8026–41.

513   Doi: 10.1128/JVI.00787-15.

514   19.   Liang Q, Luo Z, Zeng J, Chen W, Foo SS, Lee SA, et al. Zika Virus NS4A and NS4B

515   Proteins Deregulate Akt-mTOR Signaling in Human Fetal Neural Stem Cells to Inhibit

516   Neurogenesis and Induce Autophagy. Cell Stem Cell. 2016;19(5):663–71. Doi:

517   10.1016/j.stem.2016.07.019.

518   20.   Heaton NS, Perera R, Berger KL, Khadka S, LaCount DJ, Kuhn RJ, et al. Dengue virus

519   nonstructural protein 3 redistributes fatty acid synthase to sites of viral replication and

520   increases cellular fatty acid synthesis. Proc Natl Acad Sci. 2010;107(40):17345–50. Doi:

521   10.1073/pnas.1010811107.

522   21.   Jordan TX, Randall G. Dengue Virus Activates the AMP Kinase-mTOR Axis To Stimulate

523   a Proviral Lipophagy. J Virol. 2017;91(11):e02020-16. Doi: 10.1128/JVI.02020-16.

524   22.   Lennemann NJ, Coyne CB. Dengue and Zika viruses subvert reticulophagy by NS2B3-

525   mediated cleavage of FAM134B. Autophagy. 2017;13(2):322–32. Doi:

526   10.1080/15548627.2016.1265192.

527   23.   Delorme-Axford E, Morosky S, Bomberger J, Stolz DB, Jackson WT, Coyne CB. BPIFB3

528   regulates autophagy and coxsackievirus B replication through a noncanonical pathway

529   independent of the core initiation machinery. MBio. 2014;5(6):e02147.

530 24. Bramley JC, Drummond CG, Lennemann NJ, Good CA, Kim KS, Coyne CB. A Three-

531   Dime1. Bramley JC, Drummond CG, Lennemann NJ, Good CA, Kim KS, Coyne CB. A

532   Three-Dimensional Cell Culture System To Model RNA Virus Infections at the Blood-

533   Brain Barrier. mSphere. 2017;2(3):e00206-17. doi:10.1128/mSphere.00206-17.

534 25. Bayer A, Lennemann NJ, Ouyang Y, Bramley JC, Morosky S, Marques ETDA, et al. Type

535   III Interferons Produced by Human Placental Trophoblasts Confer Protection against Zika

536   Virus Infection. Cell Host Microbe. 2016;19(5):705–12. Doi: 10.1016/j.chom.2016.03.008.

537 26. Morosky S, Lennemann NJ, Coyne CB. BPIFB6 Regulates Secretory Pathway Trafficking

538   and Enterovirus Replication. 2016;90(10):5098–107.

539 27. Kamiyama D, Sekine S, Barsi-Rhyne B, Hu J, Chen B, Gilbert LA, et al. Versatile protein

540   tagging in cells with split fluorescent protein. Nat Commun. 2016;7:11046.

541 28. Kerppola TK. Bimolecular fluorescence complementation (BiFC) analysis as a probe of

542   protein interactions in living cells. Annu Rev Biophys. 2008;37:465–87.

543 29. Yu C-Y, Hsu Y-W, Liao C-L, Lin Y-L. Flavivirus Infection Activates the XBP1 Pathway of

544   the Unfolded Protein Response To Cope with Endoplasmic Reticulum Stress. J Virol.

545   2006;80(23):11868–80. Doi: 10.1128/JVI.00879-06.

546 30. Datan E, Roy SG, Germain G, Zali N, McLean JE, Golshan G, et al. Dengue-induced

547   autophagy, virus replication and protection from cell death require ER stress (PERK)

548   pathway activation. Cell Death Dis. 2016;7(3):e2127.

549 31. Aktepe TE, Liebscher S, Prier JE, Simmons CP, Mackenzie JM. The Host Protein

550   Reticulon 3.1A Is Utilized by Flaviviruses to Facilitate Membrane Remodelling. Cell Rep.

551   2017;21(6):1639–54. Doi: 10.1016/j.celrep.2017.10.055.

552 32. Grumati P, Morozzi G, Hölper S, Mari M, Harwardt M-LI, Yan R, et al. Full length RTN3

553   regulates turnover of tubular endoplasmic reticulum via selective autophagy. Elife.

554   2017;6:e25555. Doi: 10.7554/eLife.25555.

555   33.   Fumagalli F, Noack J, Bergmann TJ, Presmanes EC, Pisoni GB, Fasana E, et al.

556   Translocon component Sec62 acts in endoplasmic reticulum turnover during stress

557   recovery. Nat Cell Biol. 2016;18(11):1173–84.

558   34.   Wong J, Zhang J, Si X, Gao G, Mao I, McManus BM, et al. Autophagosome Supports

559   Coxsackievirus B3 Replication in Host Cells. J Virol. 2008;82(18):9143–53. Doi:

560   10.1128/JVI.00641-08.

561   35.   Harris KG, Morosky SA, Drummond CG, Patel M, Kim C, Stolz DB, et al. RIP3 regulates

562   autophagy and promotes coxsackievirus B3 infection of intestinal epithelial cells. Cell

563   Host Microbe. 2015;18(2):221–32. Doi: 10.1016/j.chom.2015.07.007.

564   36.   Wu H, Zhai X, Chen Y, Wang R, Lin L, Chen S, et al. Protein 2B of coxsackievirus B3

565   induces autophagy relying on its transmembrane hydrophobic sequences. Viruses.

566   2016;8(5):1–11.

567   37.   Mateo R, Nagamine CM, Spagnolo J, Mendez E, Rahe M, Gale M, et al. Inhibition of

568   Cellular Autophagy Deranges Dengue Virion Maturation. J Virol. 2013;87(3):1312–21.

569   Doi: doi/10.1128/JVI.02177-12.

570   38.   Bingle CD, Craven CJ. PLUNC: a novel family of candidate host defence proteins

571   expressed in the upper airways and nasopharynx. Hum Mol Genet. 2002;11(8):937–43.

572   39.   Bingle CD, LeClair EE, Havard S, Bingle L, Gillingham P, Craven CJ. Phylogenetic and

573   evolutionary analysis of the PLUNC gene family. Protein Sci. 2004;13(2):422–30.

574   40.   Bingle CD, Seal RL, Craven CJ. Systematic nomenclature for the

575   PLUNC/PSP/BSP30/SMGB proteins as a subfamily of the BPI fold-containing

576   superfamily. Biochem Soc Trans. 2011;39(4):977–83.

577   41.   Wang S, Tukachinsky H, Romano FB, Rapoport TA. Cooperation of the ER-shaping

578   proteins atlastin, lunapark, and reticulons to generate a tubular membrane network. Elife.

579   2016;5(September):1–29.

580   42.   Fang YT, Wan SW, Lu YT, Yao JH, Lin CF, Hsu LJ, et al. Autophagy facilitates antibody-

581   enhanced dengue virus infection in human pre-basophil/mast cells. PLoS One.

582   2014;9(10):1–10.

583   43.   Medina F, Medina JF, Colon C, Vergne E, Santiago GA, Munoz-Jordan JL. Dengue virus:

584   Isolation, propagation, quantification, and storage. Curr Protoc Microbiol.

585   2012;(SUPPL.27):1–24.

586   44.   Payne AF, Binduga-Gajewska I, Kauffman EB, Kramer LD. Quantitation of flaviviruses by

587   fluorescent focus assay. J Virol Methods. 2006;134(1–2):183–9.

588   45.   Coyne CB, Bergelson JM. Virus-induced Abl and Fyn kinase signals permit

589   coxsackievirus entry through epithelial tight junctions. Cell. 2006;124(1):119–31.

590   46.   Delorme-Axford E, Donker RB, Mouillet J-F, Chu T, Bayer A, Ouyang Y, et al. Human

591   placental trophoblasts confer viral resistance to recipient cells. Proc Natl Acad Sci.

592   2013;110(29):12048–53. Doi: 10.1073/pnas.1304718110.

593   47.   Love MI, Huber W, Anders S. Moderated estimation of fold change and dispersion for

594   RNA-seq data with DESeq2. Genome Biol. 2014;15(12):550. Doi: 10.1186/s13059-014-

595   0550-8.

596

597   **Figures**

598
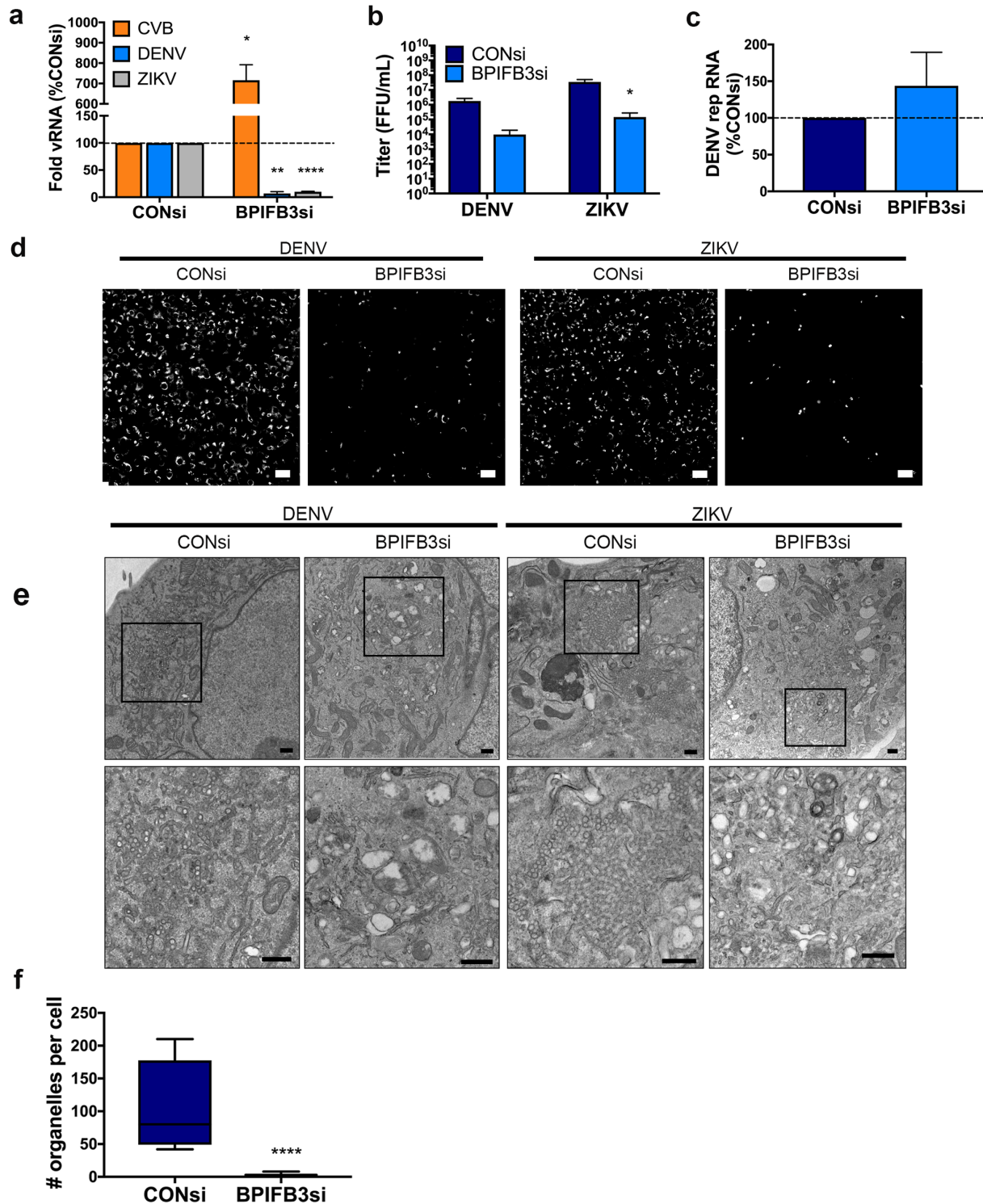
**Figure 1. BPIFB3 depletion restricts an early step in flavivirus infection**. **(a)** Infection levels of CVB, DENV, and ZIKV determined by RT-qPCR. Data are presented as a percent change from CONsi-transfected cells. **(b)** Titration (by fluorescence focus unit assay) of DENV and ZIKV

602   infectious particle production from HBMEC from panel (a). **(c)** DENV replicon RNA levels as

603   determined by RT-qPCR in response to BPIFB3 depletion, presented as percent of CONsi. **(d)**

604   Immunofluorescence microscopy for dsRNA (green), a replication intermediate, in CONsi or

605   BPIFB3si transfected HBMEC. Scale bar is 50 μm. **(e)** TEM from HBMEC transfected with CONsi

606   or BPIFB3si and infected with DENV or ZIKV. Top panel scale bar is 2 μm and bottom panel scale

607   bar is 500 nm. **(f)** Quantification of the number of ZIKV replication organelles per cell in TEM

608   images (panel e). Students t test were performed to determine statistical significance (*< 0.05, **

609   < 0.01, *** < 0.001, **** < 0.0001).
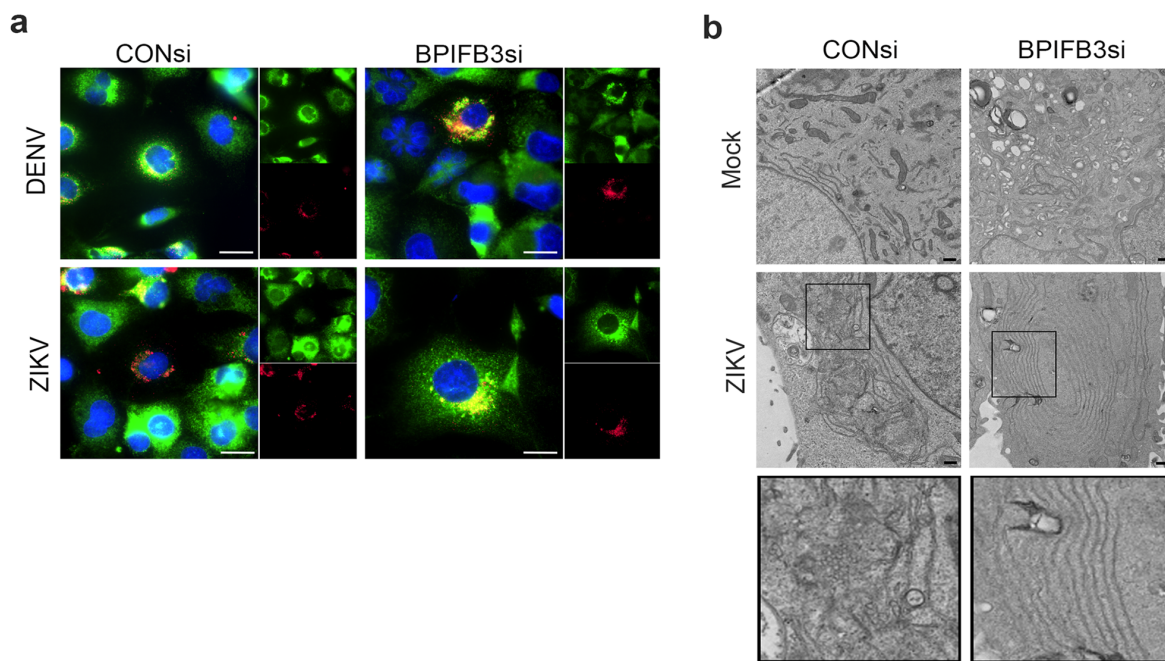
610

611   **Figure 2. BPIFB3 depletion induces aberrant ER structures during flavivirus infection**. **(a)**

612   Immunofluoresence microscopy from CONsi or BPIFB3si transfected HBMEC infected with DENV

613   or ZIKV (MOI=1) and stained for dsRNA (red) and Climp63 (green) 48hrs post-infection. Scale

614   bars are 20 μm. **(b)** TEM images from CONsi or BPIFB3si transfected HBMEC infection with ZIKV

615   (or mock infected controls). Scale bars are 2 μm.

616

617
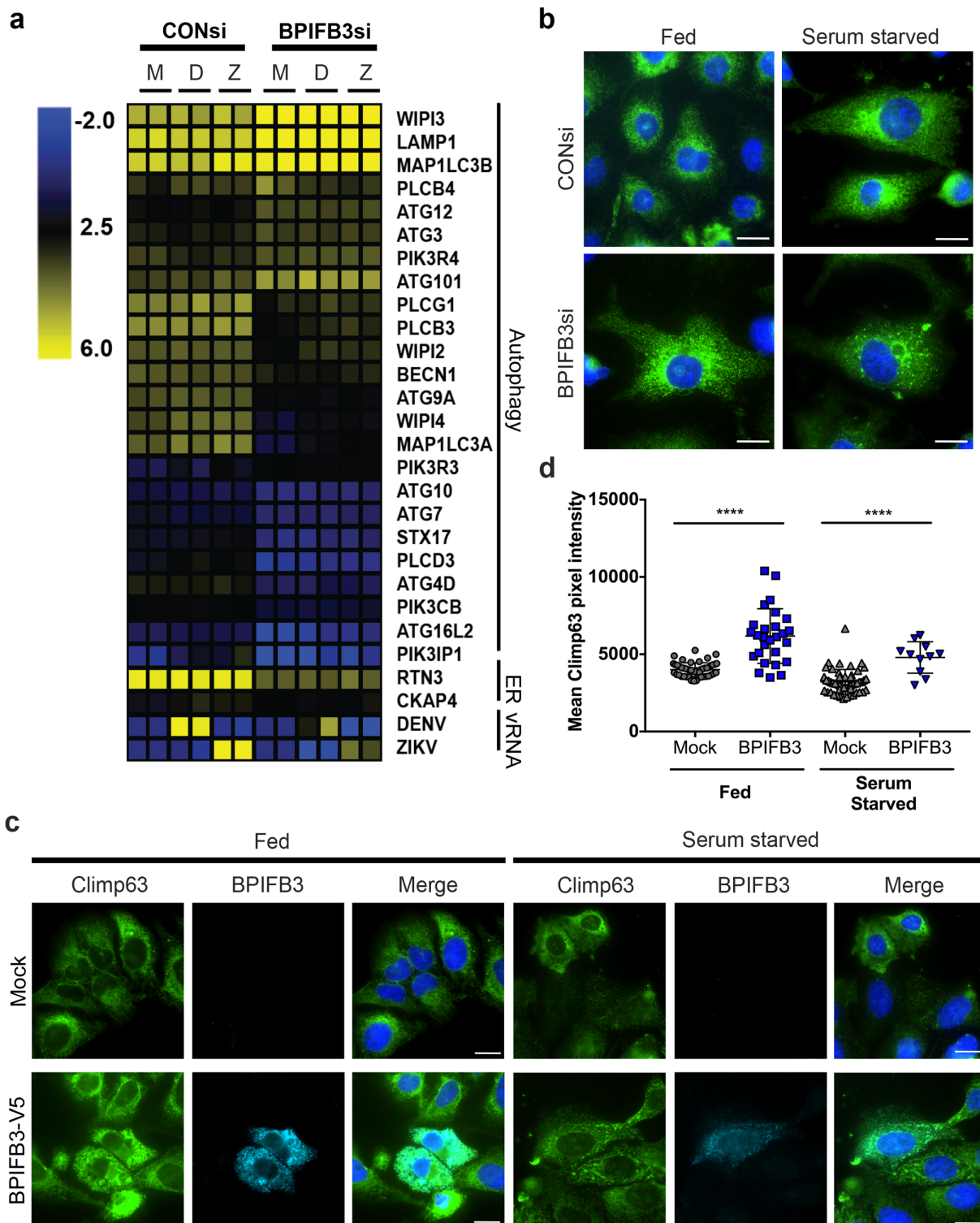
Figure 3. BPIFB3 controls ER turnover through an autophagy-associated pathway. **(a)**

Heatmap of $\log_2$(RPKM) values as determined by RNASEq from mock (M), DENV (D), or ZIKV

620   (Z)-infected CONsi and BPIFB3si transfected HBMEC. **(b)** Climp63 (green) ER morphology of

621   CONsi and BPIFB3si HBMECs under fed and serum starved conditions. **(c)** U2OS cells

622   expressing BPIFB3-V5 or Mock transfected were either fed or serum starved and stained for

623   Climp63 (green) and V5 (teal). **(d)** Quantification of Climp63 pixel intensity from panel c shows

624   BPIFB3 expression corresponds to increased levels of the ER sheet marker. All scale bars are

625   20 μm. A non-parametric Kruskal-Wallis test was performed to determine significance of IF pixel

626   quantification (**** < 0.0001).

27

627
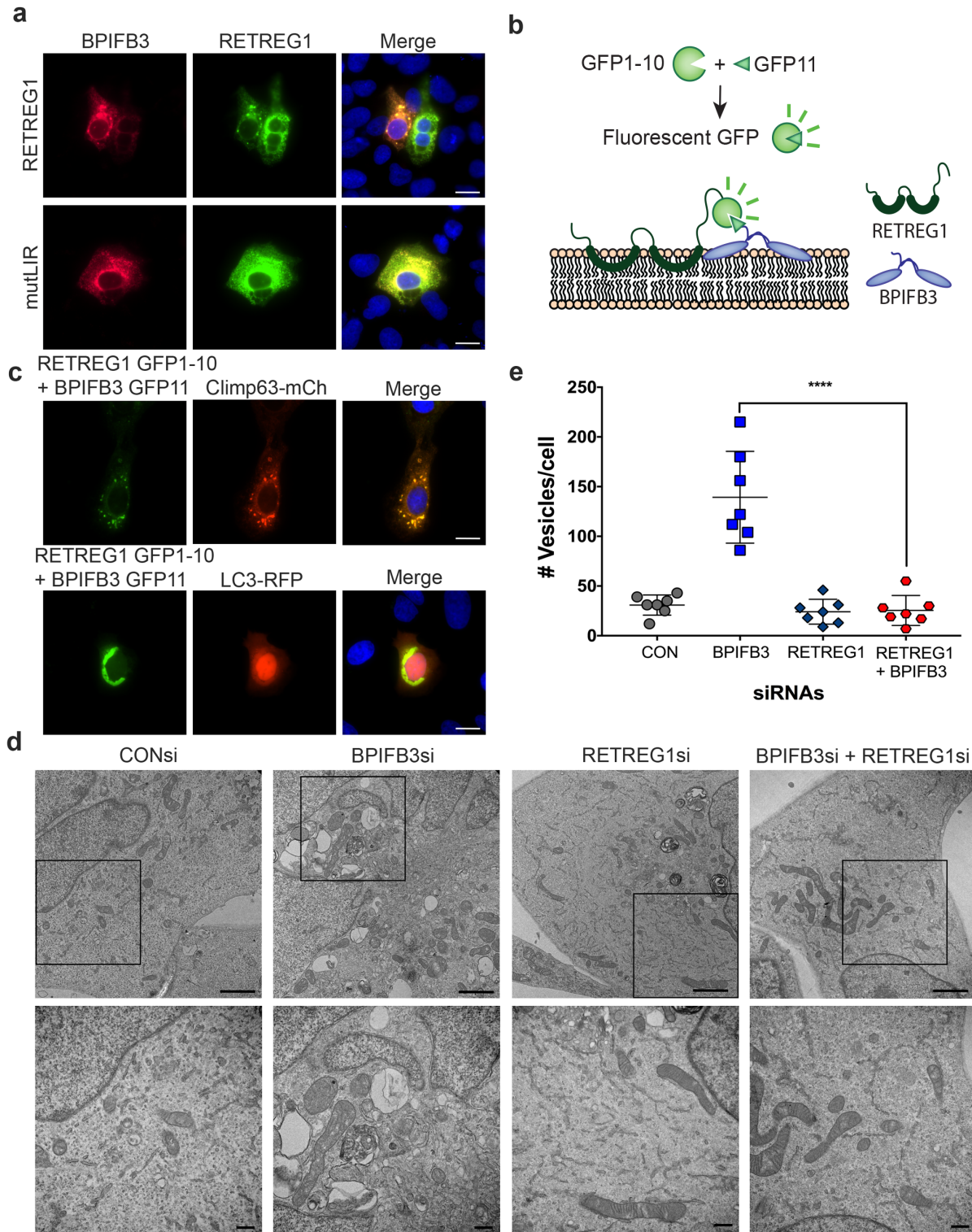
Figure 4. BPIFB3 and RETREG1 co-ocalize to ER sheets. **(a)** U2OS cells transfected with BPIFB3-V5 and RETREG1-GFP or RETREG1 mutLIR GFP. **(b)** Schematic of modified BiFC

628

629

630   assay using split GFP. **(c)** Split GFP assay, RETREG1 GFP1-10 and BPIFB3 GFP11 were co-

631   expressed with Climp63-mCherry or LC3-RFP. Green fluorescence indicates RETREG1 and

632   BPIFB3 are in close enough proximity to interact. Immunofluorescence scale bars are 20 μm. **(d)**

633   TEM of HBMEC depleted of BPIFB3 and RETREG1 alone or together. Top panel shows total cell

634   morphology, scale bars represent 2 μm. Black boxes indicated regions magnified in bottom panel

635   to show ER membrane and vesicle morphology. Lower panel scale bars are 500 nm. **(e)**

636   Quantification of total cytoplasmic vesicles from seven cells in each knockdown condition. A One-

637   way ANOVA was performed to determine significance (**** < 0.0001).
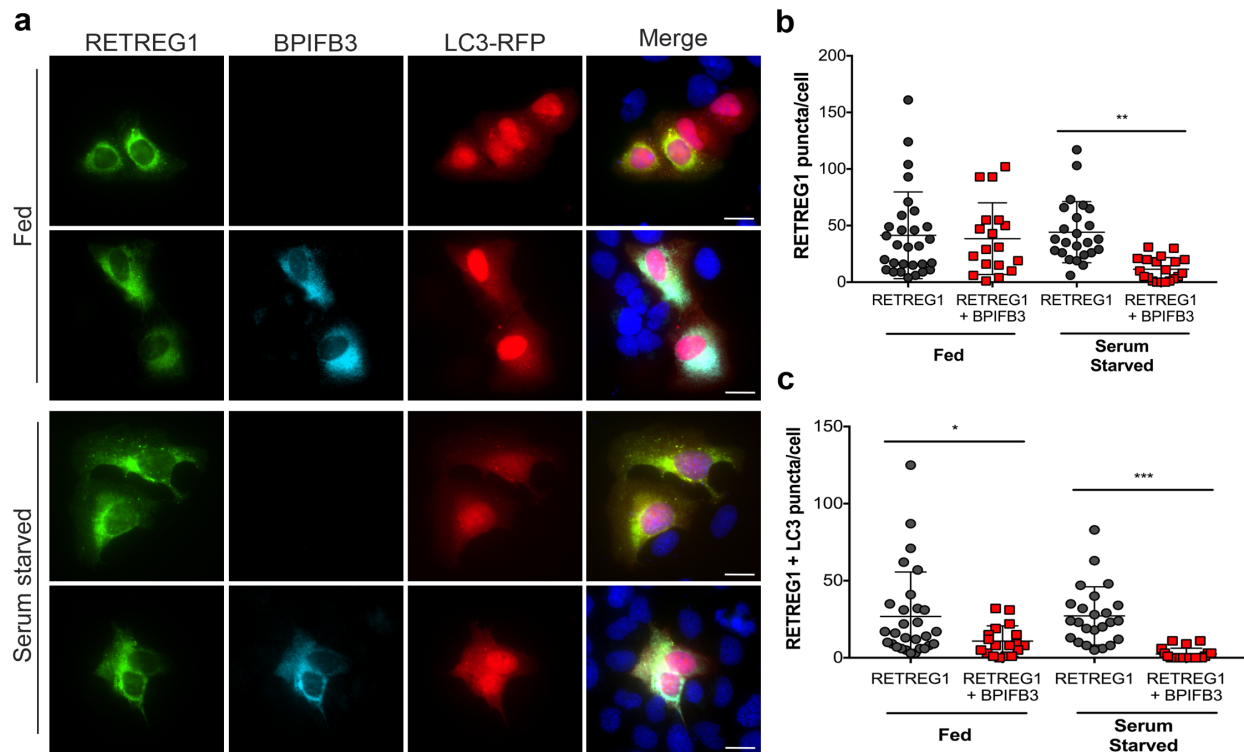
638

639   **Figure 5. BPIFB3 inhibits RETREG1 reticulophagy in response to nutrient deprivation**. **(a)**

640   U2OS cells co-expressing RETREG1-GFP and LC3-RFP were co-transfected with or without

641   BPIFB3-V5 and kept under fed or serum starved conditions. **(b)** Total RETREG1 puncta were

642   quantified under each condition as indicated. **(c)** Quantification of the number of RETREG1 and

643   LC3 positive positive puncta under either nutrient rich (fed) or nutrient deprived (serum starved)

29
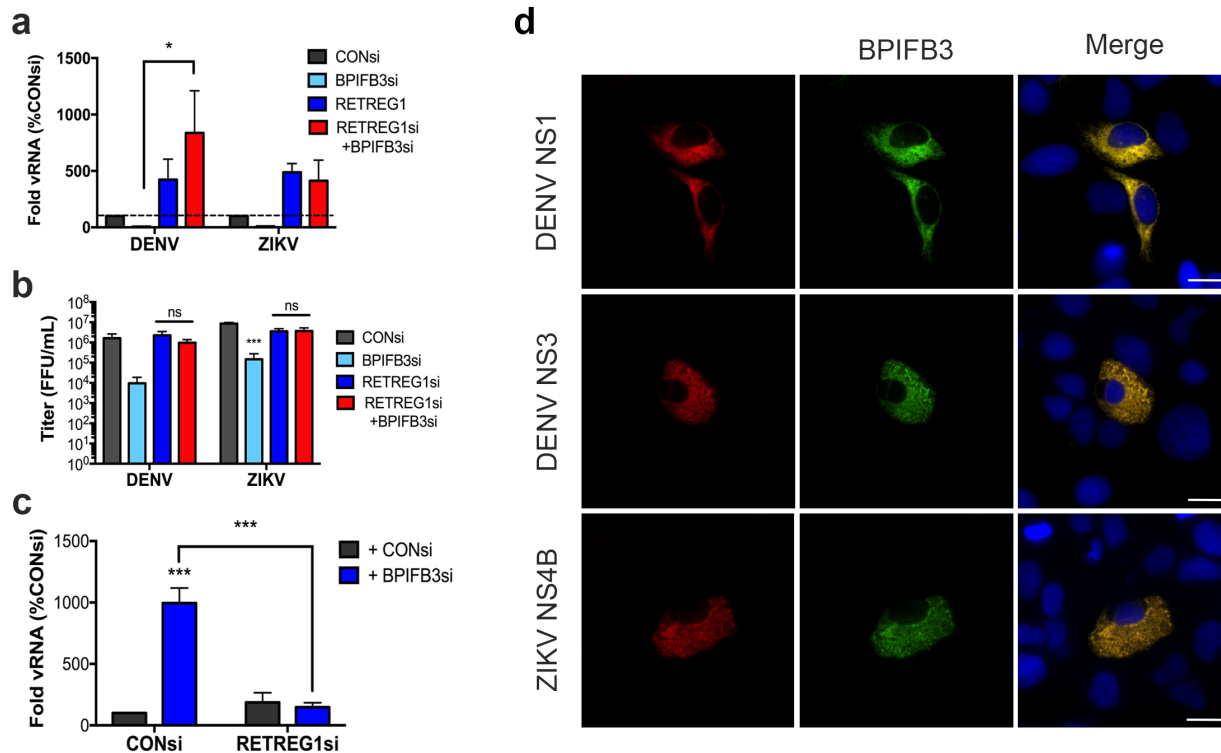
Figure 6. BPIFB3 regulates RETREG1 specific reticulophagy during flavivirus infection. **(a)** RT-qPCR for DENV and ZIKV infection levels in cells depleted of BPIFB3 and RETREG1 alone or together. **(b)** Infectious particle production from BPIFB3 and RETREG1 depleted cells as determined by fluorescence focus unit (FFU) assays. **(c)** Cells depleted of BPIFB3 and RETREG1 were infected with CVB at a MOI of 1 and analyzed for level of infection by RT-qPCR. Statistical significance was determined by 2-way ANOVA for each panel (* < 0.05, *** < 0.001). **(d)** U2OS cells overexpressing DC-SIGN to enhance infection were transfected with BPIFB3-V5 (green) and then infected with DENV or ZIKV. Cells were fixed and stained 48hrs following infection and immunostained for the indicated viral proteins (in red).